PAPER

Melting of large Pt@MgO(1 0 0) icosahedra

IOP Publishing Journal of Physics: Condensed Matter
J. Phys.: Condens. Matter **29** (2017) 145402 (7pp) https://doi.org/10.1088/1361-648X/aa5a1d

Melting of large Pt@MgO(1 0 0) icosahedra

K Rossi[1,4], T Ellaby[1,4], L O Paz-Borbón[1,2], I Atanasov[3], L Pavan[1] and F Baletto[1]

[1] Physics Department, School of Natural and Mathematical Sciences, King's College London, Strand Campus, London, WC2R 2LS, United Kingdom
[2] Instituto de Física, Universidad Nacional Autónoma de México, Apdo. Postal 20-364, 01000 Mexico, D.F. Mexico
[3] Institute of Electronics, Bulgarian Academy of Sciences, 72 Tzarigradsko Chaussee Blvd, 1784 Sofia, Bulgaria

E-mail: francesca.baletto@kcl.ac.uk

Received 21 October 2016, revised 1 December 2016
Accepted for publication 18 January 2017
Published 2 March 2017

Abstract

On the basis of *ab initio* calculations, we present a new parametrisation of the Vervisch–Mottet–Goniakowski (VMG) potential (Vervisch *et al* 2002 *Phys. Rev.* B **24** 245411) for modelling the oxide–metal interaction. Applying this model to mimic the finite temperature behaviour of large platinum icosahedra deposited on the pristine MgO(1 0 0), we find the nanoparticle undergoes two solid–solid transitions. At 650 K the 'squarisation' of the interface layer, while a full reshaping towards a fcc architecture takes place above 950 K. In between, a quite long-lived intermediate state with a (1 0 0) interface but with an icosahedral cap is observed. Our approach reproduces experimental observations, including wetting behaviour and the lack of surface diffusion.

Keywords: Pt nanoparticles, metal/oxide interaction, melting, molecular dynamics

(Some figures may appear in colour only in the online journal)

1. Introduction

Free, supported and encapsulated metallic nanoparticles (mNPs) receive a remarkable amount of interest because of their applications in various fields, ranging from nanocatalysis to biomedicine. At the nanoscale, significant surface and interface energetic contributions, together with the lack of translation symmetry in the systems, give rise to a multi-funnel energy landscape where a variety of morphologies are accessible. Hence, there is an opportunity for tuning mNPs' chemophysical properties by controlling their architecture. This possibility has stimulated a threefold research line: elucidating the correlation between shape and specific properties [1–5]; sampling the potential energy surface of a variety of morphologies to identify different motifs and equilibrium structures [6–8]; addressing the coexistence of different morphologies by understanding shape fluctuations and elucidating what rearrangement mechanism takes place [6, 9–12]. In this regard, computational tools can lead to a profound understanding of the kinetic, energetic and thermodynamics of metallic nanoparticles, thus providing an aid in a designing performant and stable ensemble of mNPs to be tested in experiments.

Previous experiments indicated that epitaxial effects dictate a shift in physical quantities, such as the melting transition, and/or the stabilisation of a phase towards another one: the thermodynamics of the nano-object can be strongly affected by the nature of its surface, e.g. exposed facets, presence of surfactants, strong interaction with the substrate [13, 14]. The melting of supported mNPs is characterised by peculiar properties such as a negative thermal expansion [15, 16], and the detection of superheated states for both free and supported clusters [16, 17]. The melting of supported metallic NPs is often limited to the case of bulk-like (FCC) shapes [18–20]. We note a single study discussed decahedral Pd on graphite, highlighting the possibility of a double melting transition with a metastable Dh cluster first melting and then recrystallising into a bulk-like (FCC) structure [21]. Up to our knowledge, no investigations relative to the thermodynamical stability of icosahedral motifs have been

[4] Authors equally contribute to the work.

reported notwithstanding this structure being often entropically and energetically favourable, especially below 4 nm, in the gas phase for a variety of noble and quasi-noble metal systems.

In this work, we propose an extension of the Vervisch–Mottet–Goniakowski (VMG) potential to allow the study of the melting of large platinum icosahedra soft-landed on the pristine MgO(1 0 0). Classical molecular dynamics (cMD) are capable of dealing with large systems (several nm in diameter), as well as finite temperatures, but require a very careful choice of the interparticle potentials and/or force fields applied. On the other hand, density functional theory (DFT) has proven successful at predicting the physico-chemical properties of nanoclusters, though it is very limited in terms of the size of the systems it can consider. Yet DFT data can still be used to fit an accurate and transferable empirical potential to be exploited in a cMD framework. To that end, producing a reliable description of the behaviour of supported nanoclusters of sizes upwards of 3 nm in diameter would greatly aid the *in silico* screening and design of next generation nanodevices. Here, we focus on the case of platinum clusters, strongly interacting with a metal oxide substrate (MgO) [22–25]. The proposed extension consists of the introduction of a smoothing function for counting the metallic coordination so to allow a dynamical description. We show that the melting of an Ih architecture is characterized by two negative specific heat peaks, as discussed in [26]. The first corresponds to the formation of a partial Ih with a (1 0 0) interface, in agreement with basin hopping calculations [27], which survives up to 900–950 K when it transforms into an FCC-like architecture. The melting transition happens well above 1500 K, which is considerably higher than in the gas phase (1300–1350 K). The structural transitions before the melting could be described as a change of the cluster surface from a spherical 'balloon' shape into a 'haystack'. The manuscript is organised as follows: after the description of the extension of the VMG potential, we outline our DFT simulations and the fitting procedure in the Methodology section; then we analyse and discuss the melting behaviour of large icosahedral clusters onto MgO(1 0 0) in the results section.

2. Methodology

To model the melting behaviour of large Pt nanoparticles deposited on an oxide surface, we propose a modification of the Vervisch–Mottet–Goniakowski (VMG) potential [28]. It is a simple and elegant energetic model firstly developed for elucidating the microscopic origin of the cohesion on Pd-oxide interface. It introduces a Morse-like function to describe the strong interaction of metal nanoparticles upon MgO(1 0 0) [27, 29–31]. This approach was successfully used for identifying the lowest energy configurations for mono and bimetallic nanoparticles supported on MgO [32–34] as well as for their solidification process [35].

In its original formulation, the energy of each metallic atom i with coordinates (x_i, y_i, z_i) and metallic coordination CN_i is given by:

$$E^i_{\mathrm{M@MgO}}(x_i, y_i, z_i, CN_i) = a_{i,1}\{e^{-2a_{i,2}(z_i - a_{i,3})} + 2e^{a_{i,2}(z_i - a_{i,3})}\},$$
$$a_{i,\alpha} = a_\alpha(x_i, y_i, CN_i), \text{ with } \alpha = 1, 2, 3 \text{ and } i \in 1, ..., N \tag{1}$$

where the number of metallic nearest neighbours within the cluster is imposed to be less than 12. The $a_{i,\alpha}$ coefficients encode both the information on the metallic coordination CN_i and the substrate geometry with respect to x_i and y_i coordinates of atom i to the substrate itself:

$$a_{i,\alpha}(x_i, y_i, CN_i) = b_{i,\alpha,1} + b_{i,\alpha,2}e^{-CN_i/b_{i,\alpha,3}}. \tag{2}$$

The periodicity of the checkerboard MgO(1 0 0) surface is reproduced by a combination of trigonometric functions in terms of the MgO lattice parameter $a = a_{\mathrm{MgO}}\sqrt{2}$,

$$b_{\alpha,\beta}(x_i, y_i) = c_{\alpha,\beta,1} + c_{\alpha,\beta,2}\left[\cos\left(\frac{2\pi}{a}x_i\right) + \cos\left(\frac{2\pi}{a}y_i\right)\right] + c_{\alpha,\beta,3}\left[\cos\left(\frac{2\pi}{a}(x_i + y_i)\right) + \cos\left(\frac{2\pi}{a}(x_i - y_i)\right)\right]. \tag{3}$$

The modelling via a VMG potential implies the fitting of the 27 parameters labelled as $c_{\alpha,\beta,\gamma}$. One should note that $c_{\alpha,3,\gamma}$ are dimensionless and they tune the screening due to the metallic coordination. On the other hand, $c_{1,1,\gamma}$ and $c_{1,2,\gamma}$ are supposed to change the strength of the interaction; $c_{3,1,\gamma}$, $c_{3,2,\gamma}$ are in Å and they control the height from the support the cluster melts it. $c_{2,1,\gamma}$ and $c_{2,2,\gamma}$, in 1 $\mathrm{Å}^{-1}$, tune the screening of the support interaction. Coefficients with $\gamma = 2, 3$ tailor the lateral contributions from the substrate.

The proposed extension of the VMG force field is intended to the study of dynamical properties of supported platinum clusters, including their melting behaviour. For avoiding any discontinuity, instead of using a sharp cutoff distance, r_c, a continuous and smooth function has been introduced to calculate the metallic coordination CN_i. Following the recipe suggested in [36], it is implemented by means of a Fermi distribution function:

$$CN_i = \sum_{j \neq i} \frac{1}{1 + \mathrm{e}^{m\left(\frac{r_{ij}}{r_c} - 1\right)}}. \tag{4}$$

The cutoff radius, r_c, and the exponent m, which tunes the smoothness of the Fermi function, are now treated as two additional parameters, and they are fitted together with the $c_{\alpha,\beta,\gamma}$ coefficients in equation (3).

The tuning of the now 27 + 2 parameters is meant to reproduce adhesion properties of a rich variety of configurations, represented by the selection of structures depicted in figure 1, as calculated by means of density functional calculations. The adhesion energy per interface atom, E_{adh}, is calculated as total energy differences between the interacting ($E_{\mathrm{M@MgO}}$) and both the relaxed gas-phase metal cluster (E_M), and MgO(1 0 0) surface (E_{MgO}) configurations:

$$E_{adh} = \frac{E_{\mathrm{M@MgO}} - (E_{\mathrm{Metal}} + E_{\mathrm{MgO}})}{N_{\mathrm{interface}}}, \tag{5}$$

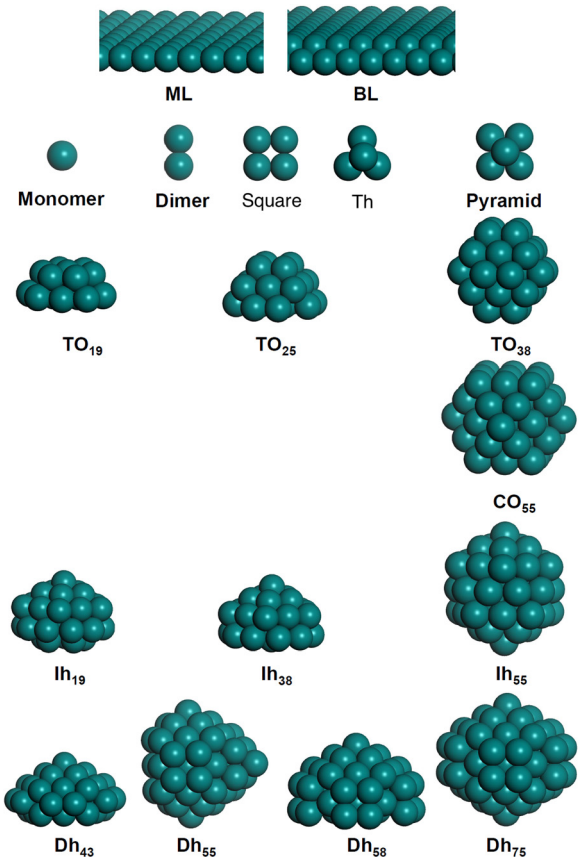

Figure 1. DFT relaxed configurations for supported Pt systems on the pristine MgO(1 0 0). The size range displayed is from monomer to 75 atoms and the mono- and bi-layer in the top row. For the sake of clarity the MgO substrate is not shown.

where negative E_{adh} values indicate favourable (exothermic) adsorption and $N_{\text{interface}}$ is the number of metallic atoms at the oxide interface.

The eighteen considered configurations range from the adatom, monolayer (ML), bilayer (BL) up to clusters with 75 atoms, shown in figure 1. They include subsets and complete shells of: (i) fcc-type truncated octahedral (TO) at sizes 19, 25 and 38 and cuboctahedral (CO), at size 55; (ii) non-crystallographic arrangements such as icosahedral (Ih) at sizes 33, 38 and 55; (iii) decahedral (Dh) at sizes 43, 55, 58 and 75. Data for each of the systems at O, Mg and hollow sites, have been included in the fitting set, following the original VMG methodology and [36]. Explicitly considering the nanoparticles landed exposing both a (1 0 0) or a (1 1 1) facet at the oxide surface. Thus having (1 1 1)-type or other type of non-commensurate interfacial geometries, accounts for several epitaxial geometries and makes the overall parametrisation more reliable in describing structural rearrangements taking place at the oxide surface.

2.1. Density functional simulations

We characterise supported Pt systems on MgO(1 0 0) via extensive DFT simulations, within the Quantum Espresso code [37]. The Perdew–Burke–Ernzerhof (PBE) approximation is used for the exchange and correlation functional term [38]. Rappe–Rabe–Kaxiras–Joannopoulos and Vanderbilt ultrasoft pseudo-potentials are used for describing Pt, Mg and O. The number of electrons treated variationally are: Pt($5d^9$ $6s^1$), Mg($2p^6$ $3s^1$ $3p^{0.75}$) and O($2s^2$ $2p^4$), respectively. Non − linear core corrections are included. A plane-wave energy and charge density cut-off of 45 Ry and 360 Ry are used. To improve convergence, a Marzari–Vanderbilt smearing parameter of 0.002 Ry is used. Structural relaxations are converged when forces are smaller than 0.001 Å eV^{-1}, with electronic total energy differences of 10^{-5} eV. The pristine surface of MgO(1 0 0) is modelled by a 6×6 supercell in a slab configuration using three atomic layers, with a lattice constant of 4.238 Å . This is marginally larger than the experimental value of 4.21 Å, though in close agreement with previous PBE calculations (4.26 Å and 4.30 Å) and hybrid PBE0 functionals (4.21 Å). [29] The size of the unit cell provides a minimum distance between lateral images of 6.5 Å, even for the largest cluster size here considered (Pt_{75}). A vacuum of 25 Å assures that the distances between images on the z-axis are located at no less than 14 Å, needed to avoid any spurious interactions between periodic images. Due to the magnetic nature of the chemical species considered, all calculations have been performed spin polarised, evaluated at the Γ-point only. The selected clusters, previously relaxed in the gas-phase, are placed onto the MgO(1 0 0) surface in order to maximise the number of Pt–O bonds, and at the initial height of 1.985 Å, optimal distance of a single Pt adatom at the O-site. Then both the slab and the cluster are relaxed. To calculate the adhesion energy per interfacial atoms, equation (5), we compare the combined Pt/MgO system with the MgO slab and the cluster in the gas-phase, using the same supercell.

Values of the DFT results are summarised in table 1, listed per cluster size and type of the facet exposed at the interlayer. Beside the adhesion energy per atom, we report some quantities to characterise the interface layer: the number of atoms at the interface $N_{\text{interface}}$, roughness of the interfacial layer, defined as the mean deviation from the Pt/Mg-site optimal height of 2.688 Å, and contact angles (∠), defined as the angle formed between the substrate and each nanoparticle facet in contact with the MgO, average bond distance of metallic atoms of the interface layer ($d_{\text{interface}}$) are reported.

An influence of dispersion effects on adhesion energies has been recently reported for supported Pt clusters over graphene [39]. Single-point calculations are performed on the relaxed configurations to account for dispersion effects using the semi-empirical approach proposed by Grimme [40]. We observe an overall increase in the adhesion energy values, from 0.34 to 0.67 eV for the ultra-nano Pt clusters (dimer to pentamer), and from 0.71 to 1.28 eV for sizes above 19 atoms. However, the general trends of the adhesion energy is maintained and most importantly the relaxed cluster shapes are not found to be significantly affected by that correction. Therefore, dispersion forces have not been taken into account further.

2.2. Parametrisation and validation of the VMG force field

The 27 coefficients in equation (3) are fitted to reproduce the DFT adhesion energy, E_{adh} (equation (5)). The Pt–Pt interaction is modelled within a second moment approximation

Table 1. *Ab initio* structural characterisation of Pt_N clusters supported on the pristine MgO(1 0 0) surface, with N number of atoms in the cluster, roughness σ, range of values for contact angle $\angle$, average Pt–Pt bond at the interface, $d_{\text{interface}}$ in Å. Last column refers to the adhesion energy per interfacial atom, E_{ads} (in eV), as defined in equation (5).

Pt_N/shape	Interface	σ	$N_{\text{interface}}$	Contact angle ($\angle_{\text{min}}/\angle_{\text{max}}$)	$d_{\text{interface}}$	E_{ads} (PBE)
19 TO	100	0.212	9	87°/131°	2.716	−0.67
25 TO	100	0.079	12	99°/128°	2.688	−0.66
33 Ih	111	0.284	14	90°/122°	2.720	−0.51
38 Ih	111	0.241	7	89°/109°	2.647	−0.54
38 TO	100	0.011	4	51°/53°	2.854	−0.92
38 TO	111	0.226	6	49°/92°	2.785	−0.67
43 Dh	111	0.179	10	33°/108°	2.757	−0.52
55 CO	100	0.087	9	68°/96°	2.778	−0.71
55 CO	111	0.048	6	52°/82°	2.801	−0.72
55 Ih	111	0.120	7	35°/104°	2.859	−0.84
55 Dh	100	0.067	8	60°/90°	2.809	−0.84
58 Dh	111	0.219	14	102°/117°	2.766	−0.53
75 Dh	111	0.139	8	37°/78°	2.812	−0.50

tight-binding potential, which has been extensively used for the study of free and supported nanoparticles [41, 42] and it is able to reproduce geometrical deformation/transition in Pt and Pt-alloyed clusters [12]. The adhesion energy is calculated for at least six different heights of the metallic cluster away from the substrate, and at different lateral (x,y) displacements: (1) O-site (0,0) corresponding to most metal atoms on top of oxygen; (2) Mg-site $(a/2,a/2)$ corresponding to most metal atoms on top of magnesium; (3) hollow-site $(a/2, 0)$ corresponding hollow surface site between oxygen and magnesium ions. As the optimal height changes depending on the later (x,y) position, we consider the following displacements along z : ±0.3, ±0.2, ±0.1 and 0 (O-site); 0.2 to 1.6 at 0.2 intervals (Mg-site); 0.2 to 1.0 at 0.2 intervals (hollow-site). In such a way, we make sure that the potential energy minimum is captured with a sufficient number of points on both sides. In the fitting we explicitly consider a single adatom, mono-layer, bilayer, a prism of 5 atoms and a half truncated octahedron of 25 atoms. The fitting of equation (1) is carried out using basin-hopping Monte Carlo optimisation algorithm where the coordination parameters, cut-off and smoothness in equation (4), are set r_c 3.468 Å and $m = 5$, respectively [36]. The robustness of the proposed parametrisation is checked versus the direct comparison of the adhesion energy for other architectures, where both (1 0 0) and (1 1 1) epitaxy are explicitly considered, such as the $TO_{38}^{(1\,0\,0)}$, $TO_{38}^{(1\,1\,1)}$, $CO_{55}^{(1\,0\,0)}$, $CO_{55}^{(1\,1\,1)}$, $Ih_{55}^{(1\,1\,1)}$, $Dh_{58}^{(1\,1\,1)}$ as well as $Dh_{75}^{(1\,1\,1)}$, as reported in figure 2.

The agreement between the DFT and EP level calculated adhesion energies is very good, though there are some clear exceptions, as for the $TO_{38}^{(1\,0\,0)}$ and the $TO_{38}^{(1\,1\,1)}$. They seem to be due to (i) a few interfacial atoms (only four for the former, which are symmetrically equivalent); (ii) a different deformation after relaxation at the DFT and empirical level. We observe a linear dependency in the calculated E_{ads} values as a function of the number of metallic atoms at the interface. The adhesion energy per contact atom is ∼0.6 eV. Upon relaxation,

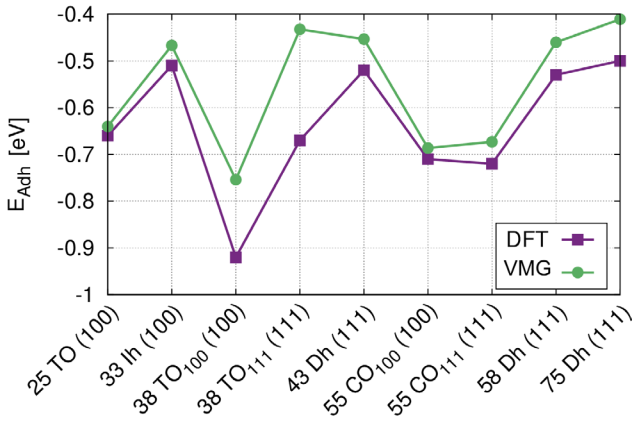

Figure 2. The adhesion energy E_{ads} per interfacial atom ($N_{\text{interface}}$) for various Pt nanoparticles depicted in figure 1 as calculated by the two levels of the theory. Per each structure, we provide the index to identify the type of the facet at the interface.

the overall gas-phase geometry of the cluster of Pt supported systems display a distribution of epitaxial configurations due to atomic rearrangements. These range from having regular atomic over-hangings (TO_{38}, CO_{55} and Dh_{55} clusters), to large contact (wetting) angles (particularly for those clusters with extended interfacial areas such as TO_{25}). Uneven over-hangings, small contact angles and several re-entrances are observed for those clusters displaying more irregular arrangements (Ih_{19} to Ih_{55}), as well as Dh_{43}, Dh_{58} and Dh_{75}). The calculated cluster average height to the substrate resembles that of monolayer (ML) cases: 2.279 Å for Pt on top of an O. Deviations from this reference value are observed for the larger cluster sizes as not all metal atoms lie on top of O-sites, and at some surface sites such as Mg, heights of nearly 2.62 Å can be expected. Our calculated bulk Pt lattice constant is 3.977 Å (cohesive energy E_{coh} value is 5.52 eV). This creates a small lattice mismatch for Pt of the order of 5%. Hence, the larger Pt–Pt bond length implies that for the vast majority of the (1 0 0) interfaces have relatively low roughness values compared to the more compact (1 1 1) ones.

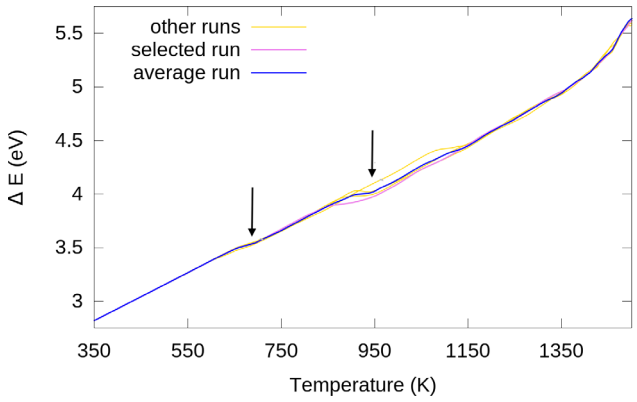

Figure 3. Caloric curves for an Ih Pt_{561} cluster: independent simulations are shown in yellow, the pink line distinguishes the run analysed in figure 4. Blue line refers to the average behaviour. The two arrows highlight the two negative specific heat transitions observed before melting.

3. Results

We probe the thermodynamic stability of Pt icosahedral clusters of 561 atoms (∼3 nm) previously relaxed in the gas phase, and then soft-landed upon a MgO(1 0 0). We adopt an iterative increasing temperature MD scheme, where the temperature, controlled by an Andersen thermostat, is increased by 50 K every 10 ns, ensuring a melting rate as slow as 5 K ns^{-1}. After a temperature increment, the system is left free to move per each temperature accordingly to Newton's equations of motion, integrated using the velocity-Verlet algorithm with a time step of 5 fs. The overall temperature range explored is 350–1500 K, although a few runs are carried out between 700–1500 K. We perform at least 7 molecular dynamics simulations to gather sensible statistics.

In figure 3 we plot the excess energy $\Delta E = E_{coh} * N = E_{pot}/N^{2/3}$, with E_{coh} is the bulk cohesive energy of the metal, E_{pot} the potential energy of the cluster and N the number of atoms, versus the mean temperature per each single run (gold lines) and their average (blue line). Referring to the average, which captures the thermodynamical behaviour of the system, we observe two transitions characterized by negative specific heat (e.g. a sharp drop in the caloric curve) around 650 K and just below 950 K. The first one ties in with the transition of the interface layer towards a (1 0 0) arrangement and a square shape while the rest of the cluster maintains an Ih architecture, the second one to the formation of a crystalline architecture, in agreement with the non continuous passage from non-crystalline to crystalline shape detected experimentally [43]. The melting transition of the cluster is instead characterised by a net departure from the linear temperature dependence of the caloric curve, which in all runs starts well after 1450 K. The melting temperature, although still lower than the Pt-bulk limit (2041 K), is about 200 K higher than those of free icosahedral Pt-nanoparticles of identical size (1300 K).

To characterize quantitatively the pre-melting structural changes we employ two geometrical descriptors. The common neighbour analysis (CNA) [44], which has been extensively used in the gas phase, enables to discriminate different atomic arrangements both in the inner and outer shells of the cluster. In particular, we look at the (5 5 5) signature which counts how many pairs of atoms belong to a five-fold axis. To have an insight on the evolution of the contour of the cluster, we slice the cluster into strips of equal height (2.37 Å) and enumerate the number of atoms in each layer. The former height is chosen as equal to the first peak of the pair distribution function multiplied by $\sqrt{(3)}/2$, which accounts for the five-fold axis being an angle of roughly 60° with respect to the pristine MgO(1 0 0) substrate.

To show in more detail how the two solid–solid transition takes place, let us focus on a specific run, figure 4. We remark that this is a paradigmatic example and similar conclusions can be obtained from all the performed simulations. Looking at the (5 5 5) signature, figure 4(a), we observe that the initial icosahedral structure is largely stable up to 650 K. Initially the Pt_{561} Ih displays 11 layers, corresponding to the number of atoms on each five-fold axis. After landing, first snapshot of figure 4(b), the base layer contains ∼20 atoms, the second layer ∼30, with a similar increase in atoms in subsequent layers until the sixth, that is the most populated, with ∼75 atoms. The number of atoms in the upper layers decreases in a similar way, figure 4(c). To some extent, this implies that the cluster shape is a 'balloon' and the contact angles of all the facets are acute obtuse on average.

In the 650–700 K temperature range, the interface layer moves to match the O-sites in the substrate as evidenced by the decrease in the (5 5 5) signature percentage, but it is still almost triangular. Hence, we observe a significant increase of the population in the first three layers at the expense of the top five ones, figure 4(c). The interface layer now has an almost square shape. In figure 4(b), we report a snapshot of the cluster just after the first structural transition, around ∼750 K: we highlight its hybrid morphology with a (1 0 0) square lowermost layer and an Ih cap.

Within 700–900 K, the upper section of the cluster shows an Ih morphology, a non-negligible (55) signature, although it decreases down to 0.5% we observe that because of the formation of (1 0 0) arrangement. We highlight that a negative heat dilation (e.g. a contraction of the first peak in the pair distribution function) is observed as long as the icosahedral cap is present, in agreement with the experimental results on similar systems [15, 16]. Above 800 K, an almost continuous increment of the population in the lower four layers, together with the loss of the upper layers is observed. A sharp increment of the 4th one and a slow constant growth of the lower ones and the contemporaneous disappearance of 5-fold symmetry axis in the clusters leads the full Ih → FCC transition, just before 950 K.

After the full solid–solid structural transition, a structurally sound cuboctahedral shape, presenting an alternation of (1 0 0) and (1 1 1) facets, is formed. Up to 1100 K, the new morphology appears stable, the few jumps in figure 4 bottom panel are either due to surface diffusion of atoms, or due to the partial reconstruction of the cluster towards a more favourable truncated octahedral architecture. These small reconstructions do not appear as significant features in the caloric curve.

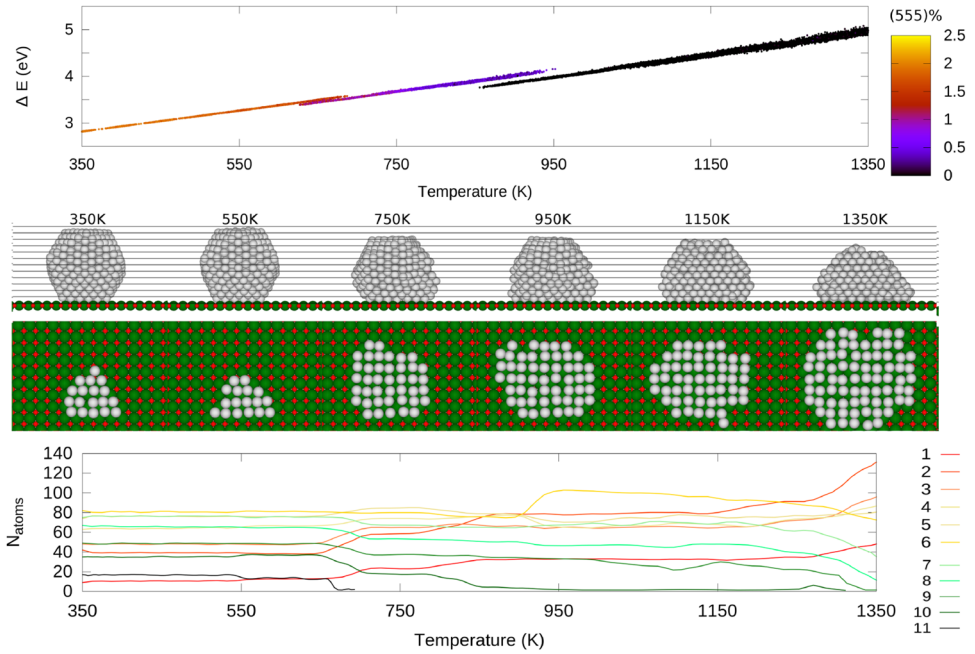

Figure 4. (a) Caloric curves for the melting simulation are reported in pink in figure 3, (5 5 5) CNA signature percentage is reported in colour with the icosahedral shape defined by a orange-red value. Dark corresponds to the absence of a five-fold axis. (b) Snapshots taken during the dynamics, Pt atoms are in grey, Mg in green and O in red. The thin lines show the striping-analysis. (c) Evolution of the number of atoms in each layer, with layer 1 being in contact with the oxide, as a function of the average temperature.

Table 2. Values of the VMG coefficient $c_{\alpha,\beta,\gamma}$ as they appear in equation (3), obtained by the fitting and used in the above study. α, β, γ runs between 1 to 3. For the coordination number the values considered are $m = 5$ and $r_c = 3.468$ Å, corresponding to a 1.25 of the Pt lattice parameter.

0.289 166	0.149 843	0.045 534
1.545 652	0.046 514	0.089 767
2.742 241	−0.261 726	−0.004 003
1.120 724	0.278 722	−0.015 515
−0.027 956	0.171 355	−0.037 242
−0.542 610	0.109 480	0.046 956
1.168 890	−0.103 545	0.033 496
2.282 238	0.655 619	0.280 348
2.093 507	−0.230 162	0.193 065

Further we note another change in the nanocluster's morphology at 1250–1300 K. Interestingly, no change/drop in the caloric curve appears for this structural transition. Above this temperature-interval, the first three layers increase their population, up to 50 atoms for the first layer and above 100 atoms for the second and the third ones. Simultaneously, we observe the loss of the two top layers as soon as the clusters melt. Around 1300 K, for the first time the second layer has more atoms than the 6th one. This change is reflected in the formation of a 'haystack' shape and it could show different wetting behaviour.

Finally, we would like to comment on the overall mobility of the Pt nanoparticles by analysing the motion of the centre of mass of the layer in contact with the oxide (COM_{base}). No changes of the COM_{base}'s coordinate are observed at low temperatures, a shift in its position of roughly one oxygen–oxygen distance is instead found at medium temperatures and a more dispersed, but still not diffusive pattern at high temperatures is reported. The cause of the shift in COM_{base} position is due to atoms originally from higher layers dropping down. The centre of mass of the whole cluster moves in the same direction, which could be explained by the mismatch between the facet of the cluster at the interface and the substrate destabilising one side of the cluster more than the others. The lack of motion is observed in all the performed simulations, we thus predict that the diffusion of large Pt icosahedra is negligible on a magnesium oxide support: even during their 'squarization' rearrangements, the center of mass shifts of one/two lattice spaces due to the enlargement of the interface facet. This can be expected due to the strong metal-oxide interaction [45, 46] and to the fact that MgO-supported Pt nanoparticles are resistant to sintering [47]. At the same time the flattening of the cluster's shape is in agreement with the experimental observation of Pt/Al_2O_3 [48].

4. Conclusion

We propose a new parametrisation for the VMG potential, as implemented in our classical molecular dynamics package. The fitting of the force-filled parameters is in order to reproduce adhesion properties obtained at *ab initio* level. Our approach enables the study of thermal and geometrical features of Pt nanoparticles in a wide size range. It is capable of reproducing experimentally observed phenomena, such as the lack of diffusion of the cluster on the oxide substrate, and its wetting to the oxide as temperature increases. We directly apply it to study the heating up to the melting of a 3 nm icosahedral Pt nanoparticle onto MgO(1 0 0). We show a fairly consistent reconstruction towards a fcc, bulk-like

arrangement, which occurs at around ∼950 K, with a melting phase transition beginning above 1500 K, roughly 200 K above the free gas melting temperature. The reconstruction of the Ih towards a FCC polyhedra agrees with energetic arguments, the latter being more favourable on an MgO(1 0 0) substrate, at least in this size range. The morphological re-arrangement is not sharp and instantaneous but it comprises intermediate and long-lived hybrid architectures, with a (1 0 0) interface and still a icosahedral upper half is observed between 700–950 K. We highlight that the intermediate architectures, named as 'squared interface + Ih', can be detected experimentally. Indeed, this shape result to be stable in a wide range of temperatures and over several tens of ns. We expect such long-lived metastable minima to be present also during other Ih into FCC transition of oxide supported metallic nanoparticles. The formation of this kind of hybrid morphology could present peculiar chemophysical properties and therefore should be considered for further applications of oxide supported Pt clusters.

4.1. Appendices

List of the new fitted parameters for Pt deposited on MgO(1 0 0).

Acknowledgments

FB, LP, LOPB thanks the financial support by UK research council EPSRC, under Grants No. EP/GO03146/1 and No. EP/J010812/1 while the studentship of KR is sponsored by EPSRC grant number ER/M506357/1. LOPB acknowledges PAPIIT-UNAM (Project IA 102716). IA and FB thanks the financial support offered by the Cost-Action MP0903 'Nanoalloy'. All the authors thanks the financial support offered by Royal Society under the project number RG120207.

References

[1] Asara G G, Paz-Borbón L O and Baletto F 2016 *ACS Catalysis* **6** 4388
[2] DiPaola C, D'Agosta R and Baletto F 2016 *Nano Lett.* **16** 2885
[3] Baletto F and Ferrando R 2015 *Phys. Chem. Chem. Phys.* **17** 28256
[4] Calle-Vallejo F, Martnez J I, Garcia-Lastra J M, Sautetand P and Loffreda D 2014 *Angew. Chem., Int. Ed.* **53** 8316
[5] Roldan Cuenya B and Behafarid F 2015 *Surf. Sci. Rep.* **70** 135
[6] Walesand D J and Doye J P K 1997 *J. Phys. Chem.* A **101** 5111
[7] Johnston R L 2003 *Dalton Trans.* **22** 4193
[8] Rossi G and Ferrando R 2009 *J. Phys.: Condens. Matter* **21** 084208
[9] Barnard A S 2010 *Rep. Prog. Phys.* **73** 086502
[10] Baletto F and Ferrando R 2005 *Rev. Mod. Phys.* **77** 371
[11] Yang Y and Zhang H 2014 *ACS Nano* **8** 7465
[12] Pavan L, Rossi K and Baletto F 2015 *J. Chem. Phys.* **143** 184304
[13] Ngandjong A C, Mottet C and Puibasset J 2016 *J. Phys. Chem.* C **120** 8323
[14] Ewing C S, Veser G, McCarthy J J, Johnson J K and Lambrecht D S 2015 *J. Phys. Chem.* C **119** 19934
[15] Vila F D, Hayashi S T, Moore J M and Rehr J J 2016 *J. Phys. Chem.* C **120** 14883
[16] Sanchez S I, Menard L D, Bram A, Kang J H, Small M W, Nuzzo R G and Frenkel A I 2009 *J. Am. Chem. Soc.* **131** 7040
[17] Gan C, Chuanjie W and Peng Z 2015 *Phys. Chem. Liq.* **53** 518
[18] Mottet C, Goniakowski J, Baletto F, Ferrando R and Treglia G 2004 *Phase Transit.* **77** 101
[19] Ding F, Rosen A, Curtarolo S and Bolton K 2006 *Appl. Phys. Lett.* **88** 133110
[20] Hendy S C 2007 *Nanotechnology* **18** 175703
[21] Schebarchov D, Hendy S C and Polak W 2009 *J.Phys.: Condens. Matter* **21** 144204
[22] Frenkel A I, Small M W, Smith J G, Nuzzo R G, Kvashnina K O and Tromp M 2013 *J. Phys. Chem.* C **117** 23286
[23] Han Y, Ferrando R and Li Z 2014 *J. Phys. Chem. Lett.* **5** 131
[24] Carrasco E, Brown M A, Sterrer M, Freund H J, Kwapien K, Sierka M and Sauer J 2010 *J. Phys. Chem.* C **114** 18207
[25] Wang H, Tobin R G, Lambert D K, DiMaggio C L and Fischer G B 1997 *Surf. Sci.* **372** 267
[26] Berry S 2004 *Israel J. Chem.* **44** 211
[27] Ferrando R, Rossi G, Levi A C, Kuntova Z, Nita F, Jelea A, Mottet C, Barcaro G, Fortunelli A and Goniakowski J 2009 *J. Chem. Phys.* **130** 174702
[28] Vervisch J W, Mottet C and Goniakowski J 2002 *Phys. Rev.* B **65** 245411
[29] Vervisch J W and Mottet C 2010 *Phys. Rev.* B **81** 155443
[30] Kozlov S M, Aleksandrov H A, Goniakowski J and Neyman K M 2013 *J. Chem. Phys.* **139** 084701
[31] Sao-Joao S, Giorgio S, Mottet C, Goniakowski J and Henry C R 2006 *Surf. Sci.* **600** L86
[32] Ferrando R, Barcaro G and Fortunelli A 2009 *Phys. Rev. Lett.* **102** 216102
[33] Goniakowski J *et al* 2009 *J. Chem. Phys.* **130** 174703
[34] Olander J, Lazzari R, Jupille J, Mangili B and Goniakowski J 2007 *Phys. Rev.* B **76** 075409
[35] Jelea A, Mottetand C, Goniakowski J, Rossiand G and Ferrando R 2009 *Phys. Rev.* B **79** 165438
[36] Atanasov I, Barcaro G, Negreiros F R, Fortunelli A and Johnston R L 2013 *J. Chem. Phys.* **138** 224703
[37] Giannozzi P *et al* 2009 *J. Phys.: Condens. Matter* **21** 395502
[38] Perdew J P, Burke K and Ernzerhof M 1996 *Phys. Rev. Lett.* **77** 3865
[39] Ramos-Sanchez G and Balbuena P B 2013 *Phys. Chem. Chem. Phys.* **15** 11950
[40] Grimme S 2006 *J. Comput. Chem.* **27** 1787
[41] Baletto F, Ferrando R, Fortunelli A, Montalenti F and Mottet C 2002 *J. Chem. Phys.* **116** 3856
[42] Mottet C, Goniakowski J, Baletto F, Ferrando R and Treglia G 2004 *Phase Transit.* **77** 101
[43] Li L *et al* 2013 *J. Am. Chem. Soc.* **135** 13062
[44] Honeycutt J D and Andersen H C 1987 *J. Chem. Phys.* **91** 4950
[45] Freund H 2002 *Surf. Sci.* **500** 271
[46] Freund H J and Pacchioni G 2008 *Chem. Soc. Rev.* **37** 2224
[47] Wettergren K *et al* 2014 *Nano Lett.* **14** 5803
[48] Stakheev A Yu and Kustov L M 1999 *Appl. Catalysis* A **188** 3